Journal of Physics: Photonics

OPEN ACCESS

RECEIVED
17 April 2025

REVISED
3 October 2025

ACCEPTED FOR PUBLICATION
15 October 2025

PUBLISHED
6 November 2025

PAPER

Photonic quantum circuits with only synchronous directional couplers in ion-exchanged glass

Jesús Liñares[1,2], Carlos Montero-Orille[1], Xesús Prieto-Blanco[1,2,*], Javier Varela-Carballo[1,2] and Daniel Balado[3]

[1] Quantum Materials and Photonics Research Group, Optics Area, Applied Physics Department, Faculty of Physics/Faculty of Optics and Optometry, Universidade de Santiago de Compostela, Campus Vida s/n, E-15782 Santiago de Compostela, Galicia, Spain
[2] iMATUS, Institute of Materials of the University of Santiago de Compostela, Avenida do Mestre Mateo, 25, Santiago de Compostela, E-15706 Galicia, Spain
[3] Grupo de investigación en Criptología y Seguridad de la Información, Instituto de Tecnologías Físicas y de la Información Leonardo Torres Quevedo, C/ Serrano 144, E-28006 Madrid, Spain
* Author to whom any correspondence should be addressed.

E-mail: xesus.prieto.blanco@usc.es

Keywords: synchronous directional couplers, integrated phase shifters, ion-exchanged glass platform

Abstract

We show that photonic quantum circuits for implementing arbitrary SU(N) transformations can be made using only synchronous directional couplers. These simple elements provide both beam splitting and phase shifting so that, under a proper concatenation of such elements, unitary transformations of arbitrary dimension can be implemented. The circuits made in this way are robust and controllable, because only one type of element is used and the technology involved in their fabrication is very mature. We present several examples of original passive photonic circuits intended for quantum projective measurements and quantum state generation due to their interest in photonic quantum technology for quantum key distribution systems. Likewise, we have designed, fabricated, and characterized, on an ion-exchanged glass platform, different couplers, which form the basic elements or building blocks of these passive circuits highly compatible with optical fibres.

1. Introduction

Integrated optics is a versatile technology used to implement devices for classical and quantum information processing. In the quantum realm, integrated optics/photonics contributes to various advancements, such as linear quantum computing based on the Knill–Laflamme–Milburn protocol [1], the generation of quantum random walks [2], and the creation and measurement of states for quantum key distribution (QKD) [3,4]. The key component in these developments is the implementation of basic units which, when properly concatenated or factorized, can perform any linear transformation.

Reck *et al* [5] demonstrated in bulk optics that using beam splitters and phase shifters successive two-mode unitary operations are sufficient to implement any unitary operation in SU(N). This approach is a clever implementation of the Murnaghan factorization [6]. These results can be translated to integrated photonics by drawing an analogy between bulk beam splitters and integrated directional couplers, as well as bulk phase shifters and integrated phase shifters. Consequently, it is indeed possible to implement any unitary operation on an integrated photonic platform and, in fact, large-scale linear network demonstrations have already been reported [7]. Moreover, the ongoing interest in these unitary transformations for classical and quantum applications has led to new designs aimed at reducing the number of basic units [8], minimizing optical losses, reducing fabrication resources, and achieving simpler factorizations of unitary transformations [9]. Various applications can be implemented, including devices for linear quantum optical computation based on CNOT gates by postselection for specific purposes, such as the well-known Deutsch–Josza algorithm [10]; devices for generating and/or measuring quantum states through projective measurements [11], such as the quantum states used in QKD protocols for quantum communications; and devices for quantum optical sensing and/or quantum metrology.

According to the aforementioned results, it can be demonstrated that the basic elements of integrated photonic devices can be simple 3 dB directional couplers and phase shifters, which enable the implementation of any SU(N) transformation. Phase shifters, in particular, are essential linear quantum optical gates. They can be reconfigured using various techniques such as electro-optic or thermo-optic control. However, for specific applications as passive devices, reconfiguration is not necessary to achieve a definite phase shift. In these cases, phase shifting can be achieved by altering certain characteristics of a channel waveguide: by lengthening or shortening its optical path length (dynamic phase shifting), modifying its cover refractive index, or changing its width adiabatically. The first two strategies are directly dependent on the frequency of the light, requiring high precision in the fabrication process or subsequent readjustment. The latter strategy is more robust but typically requires long path lengths, which can limit the number of elements that can be made in the device. These are standard phase shifting strategies used in different platforms [5, 7, 11].

In this paper, we propose devices whose phase shifters are based solely on synchronous directional couplers. This approach allows any optical integrated circuit to be implemented using only these building blocks, thereby avoiding the mixture of different design strategies for integrated optical elements. Moreover, the technologies involved in the fabrication of directional couplers are very mature, and many laboratories can manufacture these elements today. It is important to emphasize that the phases obtained are either topological (geometrical) or use the slow part of the dynamic phase of the eigenstates of a directional coupler [12]. We will demonstrate that this approach is more advantageous than previous ones because it enables robust phase shifting. This constitutes one of the main results of this work. Additionally, this paper presents passive quantum devices that use only synchronous directional couplers, to achieve both power derivations and phase shifts, and thus to generate and measure quantum states for QKD protocols, such as the generalized BB84 for arbitrary dimensions [4]. These proposals will illustrate the usefulness of phase shifters, although they can be applied to many other areas.

We also present experimental results on an ion-exchanged glass platform. Ion exchange is a well-established fabrication technology [13–15] that offers several advantages over other technologies. It uses inexpensive substrates, has high compatibility with optical fibres and possesses great development potential because non-linearity can be generated in ion-exchanged glasses through poling [16] or rare-earth doping [17]. Furthermore, the ion exchange process smooths out lithographic defects smaller than the diffusion depth, thereby reducing scattering losses. While high refractive-index contrast technologies enable significant miniaturization of integrated photonic circuits, these platforms require extremely precise and costly lithography to maintain propagation losses, caused by edge scattering, at a moderate level. Such losses are particularly detrimental in quantum systems. However, unlike quantum computation and quantum processing applications, QKD protocols, such as those explored in this work, typically involve a moderate number of optical components, allowing one to take advantage of the low losses inherent to the ion-exchange platform without circuit size being a significant limitation. Therefore, a high integration is not required and even not desired for the sake of optical fibre compatibility. Our experiments were conducted in the 800–900 nm optical communication band, although they could be extended to longer wavelengths. That band allows the use of quantum optical sources and single-photon detectors that are significantly more affordable and efficient compared to those used in the 1260–1625 nm band. Moreover, both bands could be used simultaneously in existing communication networks: the former for the QKD protocols and the latter for classical communications. Although optical fibres exhibit higher losses in the wavelength range 800–900 nm, transmission of QKD protocols could be carried out over short distances.

The plan of the paper is as follows: in section 2 we show how to make phase shifters by means of 2×2 and 3×3 directional couplers. The former provide topological phases π and $\pi/2$ which are very common in many integrated optical devices. The latter provide slow dynamic phases and allow us to achieve any value. In section 3 we use these results to propose some quantum optical projectors, that is, devices to determine the QKD quantum states by projective measurements. This is done for dimensions two and four, as those required for implementing random passive measurements in QKD protocols. Likewise, random optical quantum state generators are also proposed. Section 4 is reserved for the experimental results. We have fabricated by ion exchange in glass, and a systematic control of the lithographic parameters, the main synchronous directional couplers of the circuits proposed in this work. In section 5, conclusions are presented.

2. Phase shifters based on 2×2 and 3×3 directional couplers

We present the theoretical aspects to implement arbitrary phase shifters with directional couplers. We start with the description of 2×2 couplers which are the building blocks of our circuits. Let us consider

a synchronous directional coupler between two channel guides with optical modes $e_1(x,y)$ and $e_2(x,y)$, propagation constant β and coupling constant κ. The general solution is given by

$$e(x,y,z) = \{a_1(z)\, e_1(x,y) + a_2(z)\, e_2(x,y)\}\, e^{i\beta z}. \tag{1}$$

The amplitudes $a_1(z)$ and $a_2(z)$ can be calculated by using the well-known matrix relationship, with the input amplitudes $a_1(0)$ and $a_2(0)$,

$$\begin{pmatrix} a_1(z) \\ a_2(z) \end{pmatrix} = \begin{pmatrix} \cos\theta & i\sin\theta \\ i\sin\theta & \cos\theta \end{pmatrix} \begin{pmatrix} a_1(0) \\ a_2(0) \end{pmatrix}, \tag{2}$$

where $\theta = \kappa z$. We must stress that this classical relationship is also valid for the quantum absorption operators $\hat{a}_1(z)$, $\hat{a}_2(z)$, $\hat{a}_1(0)$, and $\hat{a}_2(0)$ acting on quantum states $|L\rangle$, therefore we can write

$$\begin{pmatrix} \hat{a}_1^\dagger(0) \\ \hat{a}_2^\dagger(0) \end{pmatrix} = \begin{pmatrix} \cos\kappa z & i\sin\kappa z \\ i\sin\kappa z & \cos\kappa z \end{pmatrix} \begin{pmatrix} \hat{a}_1^\dagger(z) \\ \hat{a}_2^\dagger(z) \end{pmatrix}. \tag{3}$$

Accordingly, if we have a quantum light state of $n_{1,2}$ photons at mode $e_{1,2}(x,y)$ at $z = 0$, that is, $|L\rangle = |n_1 n_2\rangle$, then we can use the relationships $\left(\hat{a}_1^\dagger(0)\right)^{n_1}|0\rangle = \sqrt{n_1!}|n_1\rangle$ and $\left(\hat{a}_2^\dagger(0)\right)^{n_2}|0\rangle = \sqrt{n_2!}|n_2\rangle$, to obtain the quantum state at a distance z. This result can be applied to any other quantum state. From now on we use these quantum operators, although from a classical point of view they can be also used as complex amplitudes of modes $e_1(x,y)$ and $e_2(x,y)$ for classical circuits. Moreover, the linear transformation given by the matrix in equation (3) will be denoted as X_θ because it is generated by the Pauli matrix X with a weight given by the parameter θ.

2.1. Phase shifters based on one 2×2 directional coupler

A first main result for fundamental phase shifters can be obtained directly from equation (3). Let us consider an input state characterized for the vector $(1,0)^{\mathrm{T}}$, where superindex T stands for transposed, which can represent a coherent state α_1 excited in mode $e_1(x,y)$, or a single photon $|1_1\rangle$ excited in mode $e_1(x,y)$. For abrupt couplers with $\kappa z = \pi$ and $\kappa z = \pi/2$ we obtain the following final states in a vector representation:

$$\boldsymbol{v}_{z=\frac{\pi}{\kappa}} = e^{i\pi}\begin{pmatrix} 1 \\ 0 \end{pmatrix}, \quad \boldsymbol{v}_{z=\frac{\pi}{2\kappa}} = e^{i\pi/2}\begin{pmatrix} 0 \\ 1 \end{pmatrix}. \tag{4}$$

Therefore, global phases $\Phi = \pi$ and $\Phi = \pi/2$ are obtained for input state $(1,0)^{\mathrm{T}}$. Note that we get the same phases for the input state $(0,1)^{\mathrm{T}}$. Then, directional couplers $X_{\pi/2}$ and X_π can also be used as phase shifters $P_{\pi/2}$ and P_π with respect to a third waveguide. Thus, in figure 1 these abrupt directional couplers act as phase shifters implementing the quantum gates S and Z, respectively, between operators $\hat{b}_1$ and $\hat{b}_2$. Obviously, a coupler $X_{3\pi/2} = X_\pi X_{\pi/2}$ can be used as a phase shifter $P_{3\pi/2}$ and, therefore, implements a gate S^*. Now, we present a most explicit derivation of the above phases to show how they are acquired through the coupler. Let us consider an abrupt coupler in the lower arm with, in turn, one upper and one lower path or channel guide as shown figure 1, that is, with an ancillary channel guide. First of all, we must indicate that the eigenvalues of a synchronous coupler are: $\beta_1 = \beta + \kappa$ and $\beta_2 = \beta - \kappa$, and the corresponding eigenvectors (optical supermodes) are: $(1/\sqrt{2})(1,1)^{\mathrm{T}}$ and $(1/\sqrt{2})(1,-1)^{\mathrm{T}}$. If we write an arbitrary vector $(v_1, v_2)^{\mathrm{T}}$ at the input $z = 0$ of an abrupt coupler as a linear combination of their eigenvectors and use the eigenvalues to propagate the state then we obtain, at a arbitrary distance z of the coupler, the following vector $\boldsymbol{v}(z)$ of amplitudes

$$\boldsymbol{v}(z) = \frac{v_1 + v_2}{2}\begin{pmatrix} 1 \\ 1 \end{pmatrix} e^{i(\beta+\kappa)z} + \frac{v_1 - v_2}{2}\begin{pmatrix} 1 \\ -1 \end{pmatrix} e^{i(\beta-\kappa)z}. \tag{5}$$

Note that there is a common and fast phase βz (β is proportional to the frequency of light ω) which is not relevant because the channel guide in the upper arm has the same propagation constant β, and more importantly there are slower phases $\pm\kappa z$ because of the modal coupling. For a distance $z = \pi/\kappa$ we obtain the same input state but it has acquired a global phase π in the lower arm. If the input state is $(1,0)$, as required in our case, we obtain a relative phase π with respect to the guide in the upper arm. A similar description applies to the global phase $\pi/2$; however, in this case, the channel guide path undergoes a shift in the lower arm. To address this, we introduce a curved segment in each channel guide, as discussed below. In short, we see that the phase shifting comes from the modal coupling

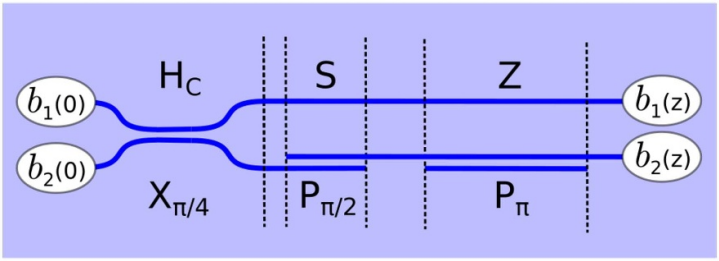

Figure 1. A quantum circuit with a non abrupt directional coupler implementing a $X_{\pi/4}$ logic gate and two phase shifters $P_{\pi/2}$ and P_π based on abrupt couplers $X_{\pi/2}$ and X_π, and therefore implementing S and Z gates, respectively.

which is characterized by a coupling coefficient $\kappa \ll \beta$ which facilitates the physical implementation of the phase shifter, that is, robust phases can be obtained.

On the other hand, in figure 1 we can also see a non-abrupt $X_{\pi/4}$ coupler at the beginning which must include some kind of curves to separate both input (and output) waveguides from each other, although this lengthens the coupler. In this case, we use four identical Minford curves [18]. This coupler ($\kappa z = \pi/4$) implements a Hadamard gate for circular states ($H_c \equiv \sqrt{iX}$) which is of a great interest in quantum processing:

$$X_{\pi/4} \equiv H_c = \frac{1}{\sqrt{2}} \begin{pmatrix} 1 & i \\ i & 1 \end{pmatrix}. \tag{6}$$

Finally we must note that the above global phases are also topological (or geometrical) [12]. They have the peculiarity of being very robust, since they change much more slowly than the dynamic phases. That is, we could choose a dynamic phase $\beta z = \pi/2$; however, due to the large value of β, it would be very difficult to get, in the fabrication process of the circuit, just the value of z necessary to obtain a phase $\pi/2$. Instead, the above phases $\pi/2$ and π depend only on the coupling constant κ which, as we will see later, is much smaller than β. Furthermore, an error in the length of these couplers does not affect the phase. For instance, if the length for obtaining a $P_{\pi/2}$ shifter has an error δz, then the output state is $\left(\epsilon, i(1-\epsilon^2/2)\right)^{\mathrm{T}}$, where $\epsilon = \kappa\delta z$. The same behaviour is true for the P_π phase shifter. Therefore, we have robust phase shifters $\pi/2$ and π.

2.2. Phase shifters based on several 2×2 directional couplers

As we have just seen, robust π, $\pi/2$, and $3\pi/2$ phase shifters are easy to achieve with one synchronous directional coupler. However, obtaining arbitrary phases requires more complex circuits. Next, we will see how to do it. Let us consider an arbitrary directional coupler, that is, $\theta = \kappa z$. Then, by using an input state $(1,1)^{\mathrm{T}}$ (eigenstate of the directional coupler), we obtain the final state

$$\boldsymbol{v}_{z=\frac{\alpha}{\kappa}} = \begin{pmatrix} \cos\theta & i\sin\theta \\ i\sin\theta & \cos\theta \end{pmatrix} \begin{pmatrix} 1 \\ 1 \end{pmatrix} = e^{i\theta} \begin{pmatrix} 1 \\ 1 \end{pmatrix}. \tag{7}$$

For expository convenience, we show in figure 2 how to get this phase shifter with 2×2 directional couplers starting from an initial state $(1,0)^{\mathrm{T}}$. The $X_{\pi/4}$ directional coupler on the left gives rise to the state $\frac{1}{\sqrt{2}}(1,i)^{\mathrm{T}}$. Next, we use a $P_{\pi/2}$ abrupt coupler ($\kappa z = \pi/2$) in the lower path to obtain the state $\frac{1}{\sqrt{2}}(1,-1)^{\mathrm{T}}$ which reaches a X_θ coupler ($\theta = \kappa z$) and therefore at the output we have $e^{-i\theta}\frac{1}{\sqrt{2}}(1,-1)^{\mathrm{T}}$. Finally, we use another $P_{\pi/2}$ abrupt coupler in the upper path and a $X_{\pi/4}$ to obtain the final state $e^{i(\pi-\theta)}(0,1)^{\mathrm{T}}$. We must stress that the location of the $P_{\pi/2}$ couplers in the lower and upper arms makes sure the equality of the dynamic phase βz of the modes. We will return on this important question in section 3. On the other hand, note that if $\theta = 3\pi/4$, that is, if we have a central coupler $X_{3\pi/4}$, then a T gate is implemented, which is also of a great interest in quantum processing. Anyway, the main drawback of this circuit is that it requires five steps, which may make it too long, therefore in the next subsection we will present an alternative solution by using 3×3 directional couplers that will only require three steps.

Finally, we give a short discussion on the possibility to apply the above approach to other quantum platforms such as superconducting quantum circuits or optical-atomic quantum circuits [19] which can be discussed jointly since microwave circuits with Josephson junctions can be considered as artificial

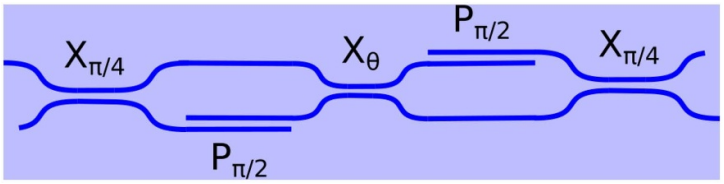

Figure 2. Integrated optical circuit to generate a phase $\Phi = \theta$. It is formed by two $X_{\pi/4}$ couplers, a X_θ coupler, and two abrupt couplers $P_{\pi/2}$. See the detailed explanation in the text.

atoms. Although these platforms have their own approachs to get phase gates we show how the above photonic approach can be implemented. For that we consider three levels in the transmon [20] and in the atom. The third level is an ancillary level to implement a phase in the second level, and therefore a relative phase with respect to the first (fundamental state). We start from the fact that the matrix solution for a transmon or an atom in resonance under the action of an external field (a Θ-pulse), which couples the second and third level, is given by the following temporal matrix

$$\begin{pmatrix} \cos\theta(t) & ie^{i(\pi+\varphi)}\sin\theta(t) \\ ie^{i(\pi-\varphi)}\sin\theta(t) & \cos\theta(t) \end{pmatrix} \tag{8}$$

where φ is the initial phase of the pulse used (which has not counterpart in the integrated photonic platforms) and $\theta(t) = \Omega t/2 = \Theta/2$, with Ω the Rabi frequency. Up to constants, this frequency depends on the characteristics of either the transmon (its capacitance and inductance) or the atom (specifically the transition amplitude between energy levels), as well as on the amplitude of the Θ-pulse. This matrix is a slightly more general that the one given by equation (2), allowing us to implement a phase shifter in fewer steps. For instance, consider the qubit $(1,0)^{\mathrm{T}}$, corresponding to the second level. If we begin with a $\pi/2$-pulse with phase $\varphi = \pi/2$, we obtain the state $(1/\sqrt{2})(1,-1)^{\mathrm{T}}$. Applying an arbitrary Θ-pulse with $\varphi = 0$ yields the state $e^{i\Theta/2}(1/\sqrt{2})(1,-1)^{\mathrm{T}}$. Finally, a $\pi/2$-pulse with phase $\varphi = 3\pi/2$ brings the system back to $e^{i\Theta/2}(1,0)^{\mathrm{T}}$, effectively introducing a phase $\theta = \Theta/2$ in the second level. This results in a phase gate acting on the subspace spanned by the first and second levels. Hence, the photonic approach is applicable to these platforms, although they offer additional capabilities due to the use of external pulses; features not available in purely photonic devices.

2.3. Phase shifters based on 2×2 and 3×3 directional couplers

A more compact arbitrary phase shifter than the previous one can be obtained by combining 3×3 and 2×2 directional couplers. In particular, two 3×3 1:1 divisors (D) and one 2×2 X_θ single coupler (see figure 3). The matrix solution for the latter is given by equation (7). With respect to the former, it is easily proven that a synchronous 3×3 directional coupler with three identical waveguides and no modal coupling between the non-neighbouring guides has the following matrix solution:

$$\begin{pmatrix} \hat{a}_1(z) \\ \hat{a}_2(z) \\ \hat{z}_3(z) \end{pmatrix} = \begin{pmatrix} \frac{\cos\sqrt{2}\kappa z+1}{2} & \frac{i\sin\sqrt{2}\kappa z}{\sqrt{2}} & \frac{\cos\sqrt{2}\kappa z-1}{2} \\ \frac{i\sin\sqrt{2}\kappa z}{\sqrt{2}} & \cos\sqrt{2}\kappa z & \frac{i\sin\sqrt{2}\kappa z}{\sqrt{2}} \\ \frac{\cos\sqrt{2}\kappa z-1}{2} & \frac{i\sin\sqrt{2}\kappa z}{\sqrt{2}} & \frac{\cos\sqrt{2}\kappa z+1}{2} \end{pmatrix} \begin{pmatrix} \hat{a}_1(0) \\ \hat{a}_2(0) \\ \hat{a}_3(0) \end{pmatrix}. \tag{9}$$

To derive the above matrix solution we have to start by calculating the eigenvalues and eigenvectors of the coupling matrix of a 3×3 synchronous coupler with propagation constant β and coupling coefficient κ (coupling is only considered between neighbouring channel waveguides). The coupling matrix M of the synchronous coupler is given by

$$M = \begin{pmatrix} \beta & \kappa & 0 \\ \kappa & \beta & \kappa \\ 0 & \kappa & \beta \end{pmatrix}, \tag{10}$$

whose eigenvalues are $\beta_1 = \beta$, $\beta_2 = \beta + \sqrt{2}\kappa$ and $\beta_2 = \beta - \sqrt{2}\kappa$ and therefore with eigenvectors

$$\boldsymbol{v}_1 = \begin{pmatrix} 1/\sqrt{2} \\ 0 \\ -1/\sqrt{2} \end{pmatrix} e^{i\beta z}, \boldsymbol{v}_2 = \begin{pmatrix} 1/2 \\ 1/\sqrt{2} \\ 1/2 \end{pmatrix} e^{i\left(\beta+\sqrt{2}\kappa\right)z}, \boldsymbol{v}_3 = \begin{pmatrix} 1/2 \\ -1/\sqrt{2} \\ 1/2 \end{pmatrix} e^{i\left(\beta-\sqrt{2}\kappa\right)z}. \tag{11}$$

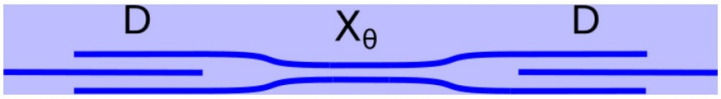

Figure 3. Integrated optical circuit generating a phase $\Phi = \theta$, formed by two divisors 1:1 implemented with 3×3 couplers and a X_θ coupler.

The asynchronous case is studied by a similar procedure, for example, in [21]. Next, we can calculate the spatial propagation of the canonical vectors and thus the columns of the matrix of equation (9) are obtained. For example, let us consider the canonical vector $(1,0,0)$, then at $z=0$ this vector is obtained by the following linear combination

$$(1,0,0) = \frac{\sqrt{2}}{2}\boldsymbol{v}_1(0) + \frac{1}{2}\boldsymbol{v}_2(0) + \frac{1}{2}\boldsymbol{v}_3(0), \tag{12}$$

therefore, the following vector is obtained at a distance z in the directional coupler

$$\left(\frac{\cos\sqrt{2}\kappa z + 1}{2}, i\frac{\sin\sqrt{2}\kappa z}{\sqrt{2}}, \frac{\cos\sqrt{2}\kappa z - 1}{2}\right), \tag{13}$$

that is, we obtain the elements of the first column of the matrix of equation (9). By using the other canonical vectors the full matrix is obtained. As commented, the asynchronous case is studied, for example, in [21, 22], which contains, as a particular case, the synchronous case.

Note that if $\sqrt{2}\kappa z = \pi/2$, then this coupler implements a divisor 1:1. Indeed, it transforms an input state $(0,1,0)^{\mathrm{T}}$ in the output state $\frac{i}{\sqrt{2}}(1,0,1)^{\mathrm{T}}$. Next, the 2×2 X_θ coupler leads to the state $e^{i(\frac{\pi}{2}+\theta)}\frac{1}{\sqrt{2}}(1,0,1)^{\mathrm{T}}$. Finally, the second coupler D transforms it into the final state $e^{i(\pi+\theta)}(0,1,0)^{\mathrm{T}}$. That is, a phase shifter $\Phi = \pi + \theta$ is obtained with three steps. Note that if the input state is $(0,-1,0)^{\mathrm{T}}$, which can be obtained with a P_π coupler, then a phase $\Phi = \theta$ is achieved.

3. Optical circuits for QKD systems

Here we show some original examples of integrated optical circuits performing QKD operations where the above solutions for phase shifting can be useful. In particular, we propose circuits for the generation and determination of the QKD quantum states, both for two and four dimensions. Detection is realized by projective measurements which is the most common procedure. We must highlight that detection and generation of quantum light states are two essential tasks in QKD.

3.1. Passive quantum projector $N = 2$ for QKD

In figure 4 we draw an integrated optical circuit for making projective measurements of states in the basis X or Y in a random way. Its operation is described in [11]. However, in that paper, no specific solution for the $\pi/2$ phase shifting is given. Our purpose here is to achieve this phase shifting by a directional coupler $P_{\pi/2}$ in the fourth waveguide, like the one shown in the previous section. The detours in the middle part of first and fourth waveguides were included so that they have the same optical paths as the second and third one, regardless of their effective indices. On the other hand, the distance between the third and fourth waveguides just after the $P_{\pi/2}$ shifter is slightly smaller than that between the first and second ones. In order the final $X_{\pi/4}$ couplers to be identical, we separated the third and fourth waveguides with two Minford curves M_{p} [18]; in addition, we also included two M_{p} curves that offset the two first waveguides but maintain their relative distance. As a result, the four outputs are equispaced and the four optical paths are equal, i.e. they have the same dynamic phase. The offset could be omitted in this particular case, but in general it allows to concatenate as many port layers as necessary by combining only a reduced set of elements. This strategy systematizes the chip design and makes easier its manufacturing because the behaviour of all couplers can be fine tuned simultaneously during the ion exchange step.

3.2. Passive quantum projector $N = 4$ for QKD

Projective measurements for higher dimensions can be made in a similar manner to that shown in the previous paragraph. For example, for dimension four, the integrated optical circuit drawn in figure 5 makes projective measurements of states in two bases in a random way [4]. A detailed description of its

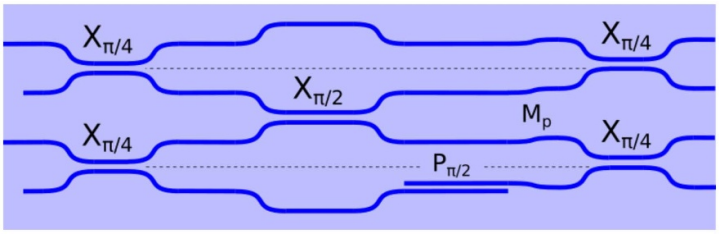

Figure 4. Drawing of an integrated quantum projector for dimension two. The $\pi/2$ phase shifting in the lower arm is achieved by an abrupt directional coupler $P_{\pi/2}$. Four Minford curves (M_p) make the four optical paths equal.

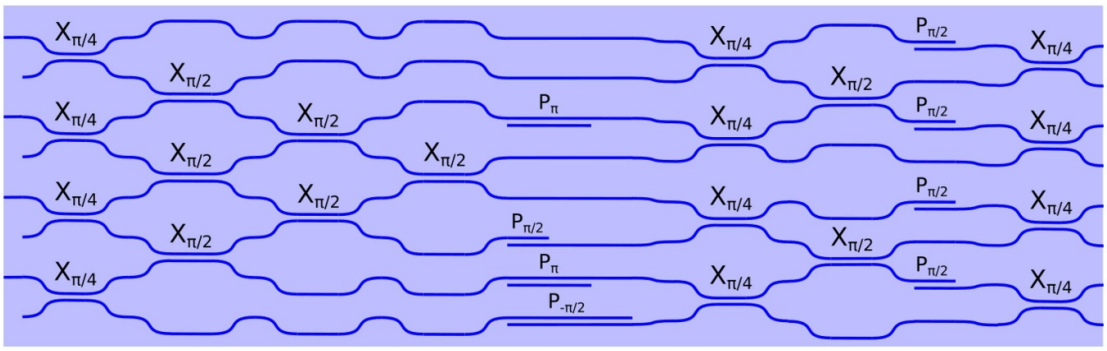

Figure 5. Drawing of an integrated quantum projector for dimension four. The phase shifting is achieved by abrupt directional couplers $P_{\pm\pi/2}$ and P_π. Again, Minford curves make the optical paths equal.

operation can be found in the previous reference. Note that, in this case, phase shifters $P_{\pi/2}$, $P_{3\pi/2}$, and P_π, implemented with abrupt synchronous directional couplers, are required together with gates $X_{\pi/4}$ and $X_{\pi/2}$ implemented with non abrupt directional couplers. The following eight states corresponding to two bases $\mathcal{B}_1$ and $\mathcal{B}_2$ can be measured, that is,

$$\mathcal{B}_1 = \left\{ \frac{1}{2}\begin{pmatrix} -1 \\ i \\ -i \\ 1 \end{pmatrix}, \frac{1}{2}\begin{pmatrix} i \\ 1 \\ 1 \\ i \end{pmatrix}, \frac{1}{2}\begin{pmatrix} 1 \\ i \\ -i \\ -1 \end{pmatrix}, \frac{1}{2}\begin{pmatrix} -i \\ 1 \\ 1 \\ -i \end{pmatrix} \right\}, \tag{14a}$$

$$\mathcal{B}_2 = \left\{ \frac{1}{2}\begin{pmatrix} -i \\ i \\ 1 \\ -1 \end{pmatrix}, \frac{1}{2}\begin{pmatrix} -1 \\ 1 \\ i \\ -i \end{pmatrix}, \frac{1}{2}\begin{pmatrix} i \\ i \\ 1 \\ 1 \end{pmatrix}, \frac{1}{2}\begin{pmatrix} 1 \\ 1 \\ i \\ i \end{pmatrix} \right\}. \tag{14b}$$

Each input vector corresponds to an output in figure 5 in descending order. The measurement is only valid when the bases of the sender and receiver match, which is checked as part of the QKD protocol.

3.3. Optical QKD quantum state generators

We will show three types of quantum state generators. One of them is an active generator where it is assumed that a quantum random number generator (QRNG) is used together with detectors and laser sources emitting weak coherent states. The other two are passive ones, one of them is based on a biphoton source and the other is based on weak coherent states by using also laser sources.

3.3.1. Active-passive quantum optical state generator

This generator can be thought as the inverse case of a quantum projector. Indeed, by inverting the circuit shown in figure 4 we obtain a generator of quantum optical states (note that $P_{\pi/2}$ commutes with $X_{\pi/2}$ located between waveguides 2 and 3). The optical circuit to generate four QKD quantum states for the BB84 protocol is shown in figure 6. It is formed by a QRNG, which is implemented in a hybrid form using an integrated circuit, four detectors, and five attenuated lasers (L_0–L_4). The laser L_0 launches pulses at single photon level in order to one of the detectors (D_1–D_4) clicks and the corresponding

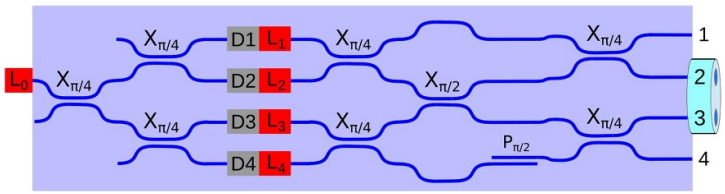

Figure 6. Integrated quantum circuit to generate the four QKD quantum states for the BB84 protocol. The circuit is assisted by a QRNG which triggers the lasers in a random way.

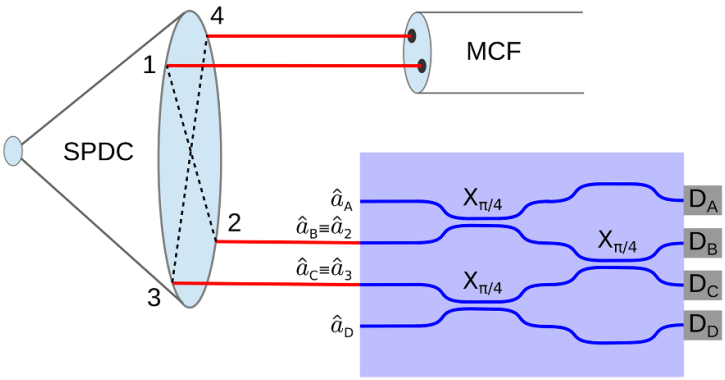

Figure 7. Passive integrated quantum circuit to generate the four QKD quantum states for the BB84 protocol by using a SPDC source of type I.

laser is triggered. This is made in a random way, because the photon coming from L_0 is in the input superposition state $|L_i\rangle = \frac{1}{2}(i|1_1\rangle + |1_2\rangle + i|1_3\rangle - |1_3\rangle)$, that is, with probability 1/4 at each input channel waveguide. Lasers L_1-L_4 are assumed to emit pulses corresponding to weak coherent states. As an example, let us consider that the QRNG triggers laser L_3, then the weak coherent state can be represented as $|\alpha_3\rangle \approx |0\rangle + \alpha_3|1_3\rangle$, that is, the laser emits a single photon with probability $|\alpha_3|^2 \ll 1$. For simplicity, we will assume that a single photon state $|1_3\rangle$ is emitted (the same result is obtained if the coherent representation $|\alpha_3\rangle$ is used). Therefore, at the end of the circuit, we get the following state (plus vacuum):

$$|L_3\rangle = \frac{1}{\sqrt{2}}\left\{ i\frac{(|1_1\rangle - |1_4\rangle)}{\sqrt{2}} - \frac{(|1_2\rangle + |1_3\rangle)}{\sqrt{2}} \right\}. \tag{15}$$

Since, the outputs 2 and 3 are coupled to a two-core optical fibre, the sent state is $|1_+\rangle = \frac{(|1_2\rangle+|1_3\rangle)}{\sqrt{2}}$, which is one of the states used in the BB84 protocol. Similarly, the state $|1_-\rangle = \frac{(|1_2\rangle-|1_3\rangle)}{\sqrt{2}}$ is obtained if the QRNG triggers the laser L_4. Finally, if the QRNG triggers L_1 and L_2, then the states $|1_L\rangle = \frac{(|1_2\rangle+i|1_3\rangle)}{\sqrt{2}}$ and $|1_D\rangle = \frac{(|1_2\rangle-i|1_3\rangle)}{\sqrt{2}}$ are, respectively, generated. Note that the probability to generate these states is 1/2, so, the 50% of the states are lost, but the rate is enough for QKD purposes.

3.3.2. Passive quantum optical state generator with spontaneous parametric down-conversion (SPDC)
A passive quantum optical state generator with SPDC is schematized in figure 7. From a light cone provided by a SPDC source of type I [23], we select four opposite points two by two. Therefore, we have a Bell state entangled in linear momentum. Next, the light from two points (1 and 4) is coupled to a two-core optical fibre (MCF) and the light from the other two (2 and 3) is coupled to the integrated device. At the outputs of this device, four single-photon detectors (D) are placed. The Bell state can be written as follows:

$$|L_B\rangle = \frac{1}{\sqrt{2}}(|1_1 1_2\rangle + |1_3 1_4\rangle). \tag{16}$$

For the sake of expository convenience, the four channel waveguides (paths) of the integrated circuit shown in figure 7 are denoted as $A, B, C, and D$), therefore the absorption operators are $\hat{a}_A$, $\hat{a}_B \equiv \hat{a}_2$,

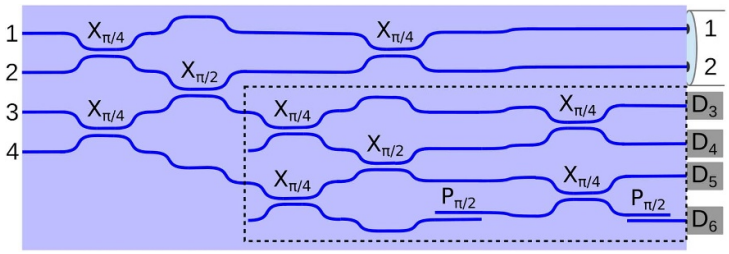

Figure 8. Passive integrated quantum circuit to generate two QKD quantum states for the B92 protocol by using two lasers at inputs 1 and 3. The part of the circuit inside a rectangle with dashed line determines the state generated.

$\hat{a}_C \equiv \hat{a}_3$ and $\hat{a}_D$. Now, by taking into account the transformations made by couplers $X_{\pi/4}$ the following output state is obtained:

$$|L\rangle = \frac{1}{\sqrt{2}}\left\{ \left[\frac{|1_A\rangle}{\sqrt{2}} - \frac{1}{\sqrt{2}}\frac{|1_B\rangle + |1_C\rangle}{\sqrt{2}}\right]|1_1\rangle + \left[\frac{|1_D\rangle}{\sqrt{2}} + \frac{1}{\sqrt{2}}\frac{|1_B\rangle - |1_C\rangle}{\sqrt{2}}\right]|1_4\rangle \right\}. \tag{17}$$

It is easy to check that four states for the BB84 protocol are obtained according to the detector triggered. For example, if detector A or D clicks then the state $|1_1\rangle$ or $|1_4\rangle$ is, respectively, obtained. These states belong to the so-called rectilinear basis. Likewise, if detector B or C clicks, we get, respectively, the state $e^{i\pi}\frac{(|1_1\rangle - |1_4\rangle)}{\sqrt{2}}$ or $e^{i\pi}\frac{(|1_1\rangle + |1_4\rangle)}{\sqrt{2}}$, which belong to the so-called diagonal basis. In this example, a phase shifter is not strictly needed except that, for some reason, the global phase $e^{i\pi}$ must be cancelled. In that case, a synchronous coupler X_π could be used in the output paths B and C to obtain a phase shift π in all the paths. Finally, note that we do not know when the state will be heralded but we do that the four states are random and with the same probability.

3.3.3. Passive quantum optical state generator with lasers

Finally, we present a passive quantum optical state generator with lasers emitting coherent states (see figure 8). The idea was originally proposed by Curty *et al* with polarization modes and bulk optics [24]. In our configuration, two laser pulses are emitted simultaneously at inputs 1 and 3 with the same photon mean value but random relative phase, that is, $|ae^{i\delta_{01}}\rangle|ae^{i\delta_{03}}\rangle$. If the difference of these phases is given by $\delta = \delta_{01} - \delta_{03} = 0, \pi/2$ then, by attenuating the outputs 1 and 2 at single-photon level (weak coherent state), we obtain two states for the B92 protocol [25]. Accordingly, the main task of this integrated circuit (Alice system) will be to determine such a phase and thus to know the quantum state sent to Bob. More in detail, the integrated circuit has six outputs. Two of them are coupled to a two-core optical fibre where the attenuation to single-photon level is made. The other four are coupled to detectors whose aim is to determine the phase δ. So, many states will lost but, as commented above, a reasonable rate of states is obtained for QKD purposes. The input state is $|L\rangle = |ae^{i\delta_{01}}\rangle|ae^{i\delta_{03}}\rangle$. It can be checked that, with the configuration proposed in figure 8, the state $|L\rangle = |\frac{a}{2}e^{i\delta_{01}}\rangle|\frac{a}{2}e^{i\delta_{03}}\rangle$ is obtained at outputs 1 and 2. This state can be approximated, under attenuation at single photon level, $a \to a' \ll 1$, by

$$|L\rangle \approx |0\rangle + \frac{a'}{2}\left[\left(e^{i\delta_{01}} - ie^{i\delta_{03}}\right)|1_1\rangle + \left(ie^{i\delta_{01}} - e^{i\delta_{03}}\right)|1_2\rangle\right]. \tag{18}$$

Therefore, for $\delta_{03} = \delta_{01}$ and $\delta_{01} - \delta_{03} = \pi/2$, two B92 states are generated, that is, states $|L_1\rangle \propto (|1_1\rangle - |1_2\rangle)$ and $|L_2\rangle \propto |1_2\rangle$.

On the other hand, the part of the circuit coupled to the four detectors (indicated inside a rectangle with dashed line in figure 8) is composed of non-abrupt directional couplers $X_{\pi/4}$ and $X_{\pi/2}$, and phase shifters $P_{\pi/2}$ implemented with abrupt couplers. It allows us to determine the value of $\delta_{03} - \delta_{01}$. Indeed, the input state is excited in channels 3 and 5 of this subcircuit and is given by $|-\frac{a}{\sqrt{2}}e^{i\delta_{01}}\rangle_3|\frac{a}{\sqrt{2}}e^{i\delta_{03}}\rangle_5$. After a long but straightforward calculation the following coherent state is obtained at the output

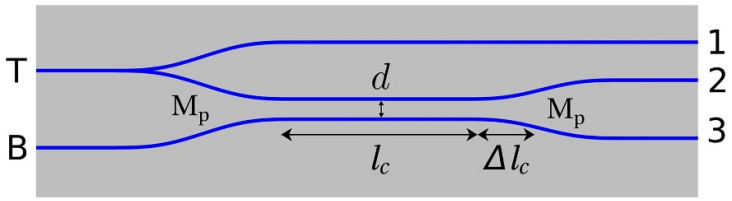

Figure 9. Basic integrated element for optical characterization purposes. M_p are the Minford curves.

channels:

$$|L\rangle = \left|\frac{-a}{2\sqrt{2}}\left(e^{i\delta_{01}} + ie^{i\delta_{03}}\right)\right\rangle_3 \left|\frac{-a}{2\sqrt{2}}\left(ie^{i\delta_{01}} + e^{i\delta_{03}}\right)\right\rangle_4 \cdot \left|\frac{a}{2\sqrt{2}}\left(e^{i\delta_{01}} - e^{i\delta_{03}}\right)\right\rangle_5 \left|\frac{-a}{2\sqrt{2}}\left(e^{i\delta_{01}} + e^{i\delta_{03}}\right)\right\rangle_6 . \tag{19}$$

Next, classical detectors measure the mean photon number or, in other words, the intensity at the outputs 3, 4, 5, and 6 which, from the last equation, is given by

$$I_{\binom{3}{4}} \propto (1 \pm \sin\delta), \; I_{\binom{5}{6}} \propto (1 \mp \cos\delta). \tag{20}$$

Therefore, for $\delta = 0$, we get $I_3 = I_4 \propto a^2$, $I_5 = 0$, and $I_6 \propto 2a^2$, and the state $|L_1\rangle$, calculated from equation (18), is excited in the two-core optical fibre. Likewise, for $\delta = \pi/2$, we get $I_3 \propto 2a^2$ and $I_4 = 0$, $I_5 = I_6 \propto a^2$, and state $|L_2\rangle$ is obtained.

4. Design, fabrication, and characterization of the basic elements of the circuits

The feasibility of the previous designs was demonstrated in an ion-exchanged glass platform [11]. This platform has been used in the past to fabricate channel waveguides and directional couplers [26, 27]. Like Albert and Yip [26], we have used a two-step thermal K^+/Na^+ ion-exchange in soda-lime glasses but, in the second step, we have buried the waveguides in order to reduce their losses and anisotropy. The parameters and details of the entire fabrication process can be found in [11]. Anyway, this process led to the manufacture of a basic integrated chip which contains 16 single directional couplers with different parameters: in particular, different coupling lengths and distances between waveguides. In the present work, we have characterized this chip for a working wavelength of $\lambda = 843$ nm which is in the first window for optical communications and is used for free-space optical links [28]. In addition, affordable semiconductor violet lasers can be used to pump a nonlinear crystal to generate quantum light states at this spectral range by spontaneous parametric down-conversion. Likewise, detection of these single photons is possible with silicon avalanche photodiodes, which are more economical than superconducting detectors used at longer wavelengths. The characterization provided us with the coupling constants and phase shifting for each coupler which allowed us to choose the appropriate couplers for the circuits shown in the previous sections.

4.1. Characterization of the chip

In figure 9 we show a drawing of the basic integrated optical element (BIOE) used for characterization. It consists of a Y-junction (top) which provides a reference signal and a directional coupler (bottom) [27].

The characterization was made using an optical system analogue to the one shown in [11]. This includes a 843 nm diode laser, a set of lenses for coupling the light to the input waveguides (T or B) of the BIOE, an eyepiece pointing at a beam splitter, so that we can see the laser pointing at the entrance, and a microscope with a camera focused on the exit face (figure 10). Through this camera, we took pictures of this exit face which allowed us to measure the output power [26]. So, measurements at outputs 2 and 3 gave us information about the characteristics of the coupler, while measurements at output 1 were useful for checking the quality of the BIOE. From the former, we estimated the relative percentage of the output power between guides 2 and 3. Knowing this power ratio, it is easy to obtain the coupling phase through the well-known synchronous directional coupler matrix [equation (2)]:

$$\theta = \kappa l_c + \kappa \Delta l_c = \arccos\sqrt{P_{\{2,3\}}/(P_2+P_3)}, \tag{21}$$

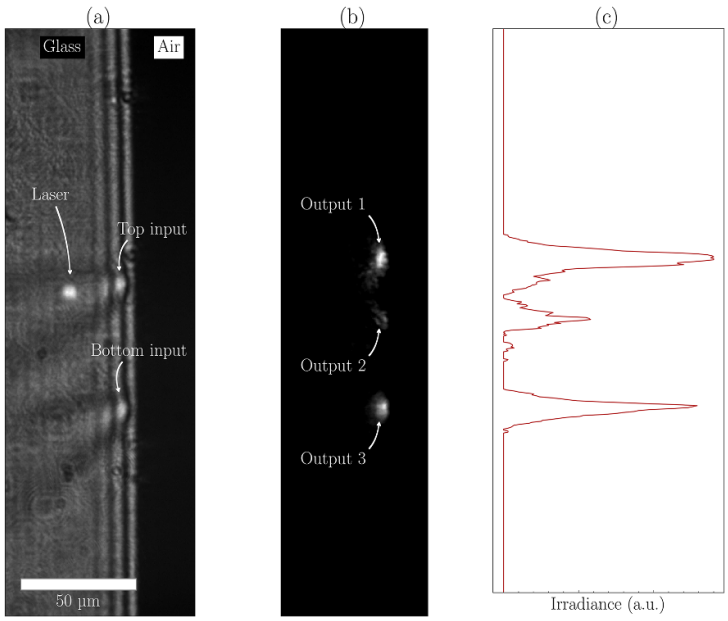

Figure 10. (a) Entrance face of the chip with red LED backlight illumination. This illumination causes fringe interferences near the transition from glass to air (like a Lloyd interferometer), as well as a bright spot on the entrance of the waveguide itself. Slightly separated to the left is the laser, which is included in the image for size reference. (b) Output face of the chip showing the waveguide outputs when the laser incides on the 'top' entrance. Image is at the same scale as (a). (c) Plot of the maximum pixel value of each row of the central image. The values of these peaks were utilized to know the power fractions of the irradiances. The images correspond to the pair $(d, l_c) = (0.5\,\text{mm}, 3\,\mu\text{m})$.

Table 1. Average power ratios (in percentages) at $\lambda = 843\,\text{nm}$: $P_2/(P_2+P_3)$ for input T and $P_3/(P_2+P_3)$ for input B.

	d (μm)			
l_c (mm)	3.0	4.5	6.0	7.5
0.5	17.36	0.00	17.30	32.04
1.0	87.74	16.40	2.60	17.93
1.5	90.30	59.50	1.76	4.40
2.0	22.51	97.54	25.60	0.03

where $P_{\{2,3\}}$ are the measured powers at the locations indicated in figure 9. Although in a straight coupler we would have only the contribution of the coupling constant κ along the length of the coupler l_c, in our directional couplers we must include another term corresponding to the contribution of the Minford curves before and after the straight part of the coupler, that is, the coupling phase gained along an effective length Δl_c.

The coupling constant is dependent on various parameters, such as wavelength or the distance between waveguides $\kappa = \kappa(\lambda, d)$. That is why, in our chip, we have 4 blocks with 4 BIOE each. So, we have 16 total elements for every combination of the coupling length $l_c = 0.5, 1, 1.5, 2$ mm and distance $d = 3, 4.5, 6, 7.5$ μm. In table 1, we show the coupling results expressed as power ratios at outputs 2 and 3 for $\lambda = 843$ nm and polarization parallel to the glass surface (vertical in figure 10). Also, in figure 10 we show a picture of the input incidence and its output measurement, along with its profile.

From these values we have calculated, through equation (21), the coupling phases. Note that this calculation has a quadrant indetermination due both the sign chosen for the square root and the arccos function. Therefore the data were unwrapped by assuming that the θ value of the shortest and widest coupler (top right value of the table 1) is in the first quadrant. Then, we have demanded that consecutive data on the table must have higher coupling, so we have increased the quadrant when that was not the case. In figure 11 we show the coupling phases obtained, as a function of the coupling length, for different separations between the waveguides of each coupler. Fits of equation (21) to these data are also shown. Thus we obtain a coupling constant k for each separation d and the basic equations which allow the selection of the right couplers for the circuits proposed in the previous section.

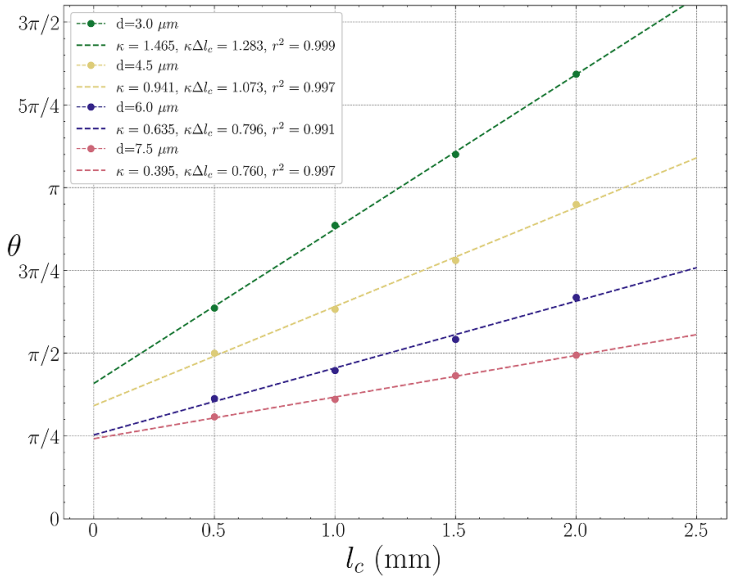

Figure 11. Coupling phase θ as a function of the coupler length l_c for four waveguide separations of the couplers d and fit of equation (21) to these data.

Table 2. Geometrical parameters for obtaining non-abrupt couplers $X_{\pi/4}$ and $X_{\pi/2}$, and abrupt couplers operating as phase shifters $P_{\pi/2}$, P_{π}, and $P_{3\pi/2}$.

Values in table: l_c (mm)					
	Coupling phase (θ)	d (μm)			
		7.5	6.0	4.5	3.0
Non-abrupt	$\pi/4$	0.06	—	—	—
	$\pi/2$	2.05	1.22	0.53	0.20
	π	6.03	3.70	2.20	1.27
	$3\pi/2$	10.01	6.17	3.87	2.34
Abrupt	$\pi/4$	1.99	1.24	0.83	0.54
	$\pi/2$	3.98	2.47	1.67	1.07
	π	7.95	4.95	3.34	2.14
	$3\pi/2$	11.93	7.42	5.01	3.22

4.2. Finding the right couplers and designing the fabrication of circuits

It is important to note that some combinations (d, l_c) of the couplers fabricated following the procedure discussed in the previous section give rise to couplers very close to the desired ones, with (7.5, 0.5), (4.5, 0.5) and (4.5, 2.0) being the closest to the phases of $\pi/4$, $\pi/2$ and π respectively. Likewise, in table 2, we show some expected combinations of (d, l_c) that lead to the desired phase shifters. Accordingly, by taking into account these empirical results on synchronous directional couplers we can design and fabricate any of the integrated devices described in section 3. As an example, consider the passive quantum projector $N = 4$ shown in figure 5. We select the following general lithographic parameters (mask feature dimensions): channel guide width $w = 3$ μm and separations of $d = 7.5$ μm and $d = 4.5$ μm between channel guides for gradual and abrupt directional couplers (phase shifters), respectively. The lithographic mask includes, on one hand, 12 gradual couplers $X_{\pi/4}$ (H_c gates) with $l_c = 0.06$ mm, 8 gradual couplers $X_{\pi/2}$ (inverters or X gates) with $l_c = 2.05$ mm, and 16 pairs of Minford curves of length $l_M = 1.52$ mm, each producing a lateral displacement of $\Delta y = 15.4$ μm. On the other hand, we lithograph 2 abrupt couplers P_{π} (Z gates) with $l_c = 3.34$ mm, 5 abrupt couplers $P_{\pi/2}$ (S gates) with $l_c = 1.67$ mm and 1 abrupt coupler $P_{-\pi/2}$ (S^* gate) with $l_c = 5.1$ mm, along with 16 Minford curves of length $l_M = 0.95$ mm, producing a displacement $\Delta y = 3.75$ μm to connect the abrupt and gradual couplers. Subsequently, a first K^+/Na^+ ion-exchange in KNO_3 is performed for 30 min at a temperature of $T = 400\,^{\circ}C$, followed by a thermal ion-exchange in $NaNO_3$ lasting 10 min to obtain buried waveguides, which reduce optical losses at the glass substrate surface. Based on the experimental results from optical characterization, the $N = 4$ projector shown in figure 5 would thus be successfully fabricated.

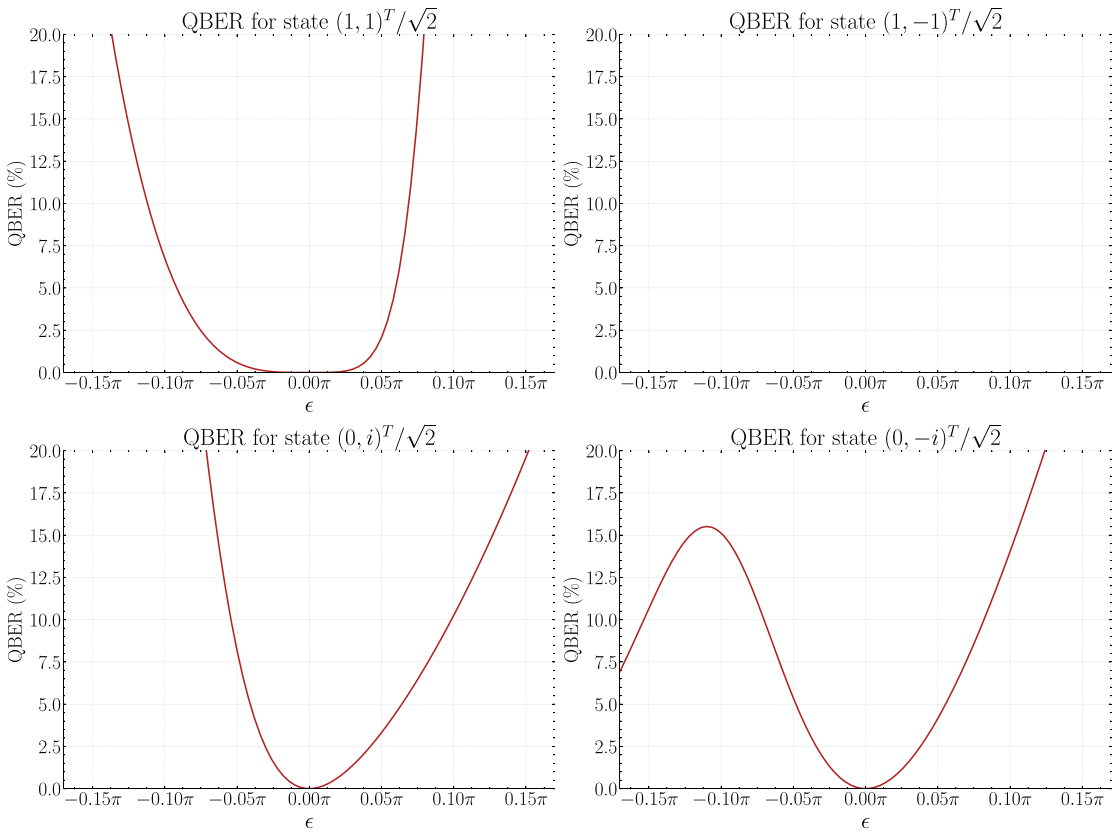

Figure 12. Quantum bit error rate of circuit of figure 4 as a function of a fabrication error ϵ in $X_{\pi/4}$ gates and 2ϵ in $X_{\pi/2}$ and $P_{\pi/2}$ gates, for each of input states of equation (22). Notably, the $(1,-1)^{\mathrm{T}}/\sqrt{2}$ state remains robust to this particular error combination.

4.3. Performance fidelity due to fabrication tolerances

In order to assess the robustness of the proposed devices against manufacturing tolerances, we will now estimate the performance degradation for the projector with $N = 2$, shown in figure 4. In this case, we select $d = 7.5\ \mu$m for both the couplers and the abrupt phase shifter $P_{\pi/2}$ ($l_c = 3.98\ \mu$m). We consider two sources of error: inaccuracies in the lithographic mask and variations introduced during the ion exchange process.

On one hand, the most critical parameter in the lithographic mask is the gap between waveguides in the couplers, which depends on the quality of the master and, primarily, on the precise control of the development of the photoresist. The latter directly impacts the waveguide width. Altogether, we encompass both errors within a tolerance of $0.25\,\mu$m in d. Note that increasing the waveguide width reduces the separation d, thereby increasing the coupling constant. However, it also raises the effective index of each waveguide, which partially offsets this increase. Accordingly, by assuming a constant waveguide width of $3\,\mu$m, we can bound the variation of the coupling constant using the fits shown in figure 11. By interpolating the fits for $d = 7.5\,\mu$m and $d = 6\,\mu$m in figure 11, we estimate that a reduction from $d = 7.5\,\mu$m to $7.25\,\mu$m results in $\kappa z = \pi(1/2 + 0.05)$ instead of $\pi/2$ in the abrupt phase shifter $P_{\pi/2}$. We reiterate that this uncertainty does not affect the phase shift itself ($\pi/2$); however, it modifies the amplitudes of the individual modes, causing part of the energy to remain in the terminating waveguide, thereby introducing losses. For simplicity, the uncertainty in κz for the gradual couplers $X_{\pi/2}$ and $X_{\pi/4}$ is assumed to be equal to and half of that of the $P_{\pi/2}$ shifter, respectively. However, these values are actually an upper bound, since the fits for $d = 7.5\,\mu$m and $d = 6\,\mu$m converge significantly for shorter couplers, taking advantage of the reduced length l_c of the gradual couplers.

On the other hand, if temperature gradients in the salt during the ion exchange process are properly controlled, a uniformity of about 1% can be achieved over several centimetres of glass surface in the difference between the effective index of the fundamental mode n_{ef} of a slab waveguide and the substrate index n_{s}, that is, $\Delta(n_{\mathrm{ef}} - n_{\mathrm{s}}) = (n_{\mathrm{ef}} - n_{\mathrm{s}})/100$. The same tolerance applies to sample repeatability. Therefore, for a given mask width, we assume that $n_{\mathrm{ef}} - n_{\mathrm{s}}$ of a channel waveguide mode can be maintained within 2% tolerance because of the two step ion-exchange process involved (waveguide formation

and burial). Considering that the coupling constant κ is proportional to $\exp(-\frac{2\pi}{\lambda}d\sqrt{n_{\rm ef}^2-n_{\rm s}^2})$, we estimate an uncertainty in the coupling constant of $\Delta\kappa \simeq 0.03\kappa$, assuming $n_{\rm ef}-n_{\rm s}\sim 10^{-3}$, a value inferred from experimental effective indices of slab waveguide regions on the same sample. Note that fine-tuning of the ion exchange process could be used to compensate for tolerances in waveguide width; however, this is not considered here.

To translate the uncertainty in the coupling constant into performance loss for the circuit in figure 4 we replace the gates $X_{\pi/4}$, $X_{\pi/2}$, and $P_{\pi/2}$ with $X_{\pi/4+\epsilon}$, $X_{\pi/2+2\epsilon}$, and $P_{\pi/2+2\epsilon}$, respectively. We then consider the four input states

$$\mathcal{B}_1=\left\{\frac{(1,1)^{\rm T}}{\sqrt{2}},\frac{(1,-1)^{\rm T}}{\sqrt{2}}\right\},\quad \mathcal{B}_2=\left\{\frac{(1,i)^{\rm T}}{\sqrt{2}},\frac{(1,-i)^{\rm T}}{\sqrt{2}}\right\} \tag{22}$$

and evaluate the quantum bit error rate (QBER), defined as the probability that the circuit measures an incorrect state within the same basis as the input, ignoring the results in the opposite basis. The results are shown in figure 12. As it can be seen, the QBER remains below 10% in all cases if $\epsilon < 0.05\pi$.

By adding the halved uncertainties from lithography (0.025π) and ion exchange (0.008π), we obtain $\epsilon = 0.033\pi$, with 2ϵ being the total uncertainty for the $P_{\pi/2}$ gates, as stated above. Therefore, the worst QBER is expected to be under a 4%. The observed limitations are not inherent to the design, but rather a direct consequence of our in-house lithographic procedure. A significant improvement is achievable by transitioning to a commercial fabrication system. Nevertheless, the aim of this work focuses on demonstrating the core concept.

5. Conclusions

Photonic quantum circuits for implementing arbitrary SU(N) transformations can be made using only synchronous directional couplers which provide both beam splitting and phase shifting. Phase shifting induced by a directional coupler is very controllable because it depends on the coupling constant of the coupler which is much smaller than the propagation constant. Integrated circuits based only on directional couplers are very robust since the technology involved in their fabrication is very mature and the use of only such building blocks avoids the mixture of different design and fabrication strategies. We have shown how to make phase shifters by means of 2×2 and 3×3 directional couplers. The former provides robust (topological) phases π and $\pi/2$ which are very common in many integrated optical devices. The latter provides very slow dynamic phases and allow us to achieve any value with a great accuracy. Due to its interest in photonic quantum technology, we have presented several examples, based only on synchronous directional couplers, of integrated passive optical circuits intended for quantum projective measurements and quantum state generation for QKD systems. This makes clear the versatility of directional couplers as building blocks for a photonic integrated circuit. Likewise, we have shown experimental results obtained on an ion-exchanged glass platform. In particular, the results about the design, fabrication, and characterization, on this platform, of the main synchronous couplers which form the basic elements of the circuits proposed in this work. Finally, we must stress that the proposals made in this work can be used in other platforms and for many other applications.

Data availability statement

All data that support the findings of this study are included within the article (and any supplementary files).

Acknowledgments

This work was supported by the MICIN, European Union NextGenerationEU under Grant PRTR-C17.I1, the Galician Regional Government through Planes Complementarios de I + D + I con las Comunidades Autónomas in quantum communication and MCIU / AEI / 10.13039/501100011033 / FEDER, UE (Project PID2023-152607NB-I00).

ORCID iDs

Jesús Liñares 0000-0002-8296-7332
Carlos Montero-Orille 0000-0003-0180-9015
Xesús Prieto-Blanco 0000-0001-7836-0143

Javier Varela-Carballo 0000-0002-1709-8601
Daniel Balado 0000-0002-0298-4598

References

[1] Knill E, Laflamme R and Milburn G 2001 A scheme for efficient quantum computation with linear optics *Nature* **409** 46–52
[2] Bian Z-H, Li J, Zhan X, Twamley J and Xue P 2017 Experimental implementation of a quantum walk on a circle with single photons *Phys. Rev. A* **95** 052338
[3] Ding Y, Bacco D, Dalgaard K, Cai X, Zhou X, Rottwitt K and Oxenlowe L K 2017 High-dimensional quantum key distribution based on multicore fiber using silicon photonic integrated circuits *npj Quantum Inf.* **3** 25
[4] Balado D, Liñares J, Prieto-Blanco X and Barral D 2019 Phase and polarization autocompensating n-dimensional quantum cryptography in multicore optical fibers *J. Opt. Soc. Am. B* **36** 2793–803
[5] Reck M, Zeilinger A, Bernstein H J and Bertani P 1994 Experimental realization of any discrete unitary operator *Phys. Rev. Lett.* **73** 58–61
[6] Murnaghan F D 1962 *Statistical Optics / Joseph W. Goodman Wiley Series in Pure and Applied Optics* (Spartan)
[7] Harris N C, Bunandar D, Pant M, Steinbrecher G R, Mower J, Prabhu M, Baehr-Jones T, Hochberg M and Englund D 2016 Large-scale quantum photonic circuits in silicon *Nanophotonics* **5** 456–68
[8] Clements W R, Humphreys P C, Metcalf B J, Kolthammer W S and Walmsley I A 2016 Optimal design for universal multiport interferometers *Optica* **3** 1460–5
[9] de Guise H, Di Matteo O and Sánchez-Soto L L 2018 Simple factorization of unitary transformations *Phys. Rev. A* **97** 022328
[10] Deutsch D and Jozsa R 1992 Rapid solution of problems by quantum computation *Proc. R. Soc. A* **439** 553–8
[11] Prieto-Blanco X, Montero-Orille C, Liñares J, González-Núñez H and Balado D 2022 Quantum projectors implemented with optical directional couplers in ion-exchanged glasses *J. Lightwave Technol.* **40** 7676–84
[12] Liñares J J and Nistal M C M C 1992 Geometric phases in multidirectional electromagnetic coupling theory *Phys. Lett. A* **162** 7–14
[13] Broquin J-E 2001 Ion-exchanged integrated devices *Integrated Optics Devices V* vol 4277, ed G C Righini and S Honkanen (International Society for Optics and Photonics, SPIE) pp 105–17
[14] Tervonen A, Honkanen S K and West B R 2011 Ion-exchanged glass waveguide technology: a review *Opt. Eng., Bellingham* **50** 071107
[15] Tellez-Limon R, Gardillou F, Coello V and Salas-Montiel R 2021 Coupled localized surface plasmon resonances in periodic arrays of gold nanowires on ion-exchange waveguide technology *J. Opt.* **23** 025801
[16] Dussauze M and Cardinal T 2019 *Nonlinear Optical Properties of Glass* (Springer) pp 193–225
[17] Righini G C and Liñares J 2021 Active and quantum integrated photonic elements by ion exchange in glass *Appl. Sci.* **11** 5222
[18] Minford W, Korotky S and Alferness R 1982 Low-loss Ti:$LiNbO_3$ waveguide bends at $\lambda = 1.3$ μm *IEEE J. Quantum Electron.* **18** 1802–6
[19] Nakahara M and Ohmi T 2008 *Quantum Computing: From Linear Algebra to Physical Realizations* (CRC Press)
[20] Koch J, Terri M Y, Jay Gambetta A A H, Schuster D I, Majer J, Alexandre Blais M H D, Girvin S M and Schoelkopf R J 2007 Charge-insensitive qubit design derived from the Cooper pair box *Phys. Rev. A* **76** 042319
[21] Burns W K and Milton A F 1988 *Waveguide Transitions and Junctions* (Springer) pp 89–144
[22] Kim C-M and Im. Y-J 2000 Switching operations of three-waveguide optical switches *IEEE J. Sel. Top. Quantum Electron.* **6** 170–4
[23] Agarwal G S 2013 *Quantum Optics* (Cambridge University Press)
[24] Curty M and Moroder T 2011 Heralded-qubit amplifiers for practical device-independent quantum key distribution *Phys. Rev. A* **84** 010304
[25] Bennett. C H 1992 Quantum cryptography using any two nonorthogonal states *Phys. Rev. Lett.* **68** 3121–4
[26] Albert J and Yip G L 1988 Wide single-mode channels and directional coupler by two-step ion-exchange in glass *J. Lightwave Technol.* **6** 552–63
[27] Walker R G and Wilkinson C D W 1983 Integrated optical waveguiding structures made by silver ion-exchange in glass. 2: directional coupler and bends *Appl. Opt.* **22** 1929–36
[28] Jurado-Navas A, Tatarczak A, Lu X, José Vegas Olmos J, María Garrido-Balsells J and Monroy I T 2015 850-nm hybrid fiber/free-space optical communications using orbital angular momentum modes *Opt. Express* **23** 33721–32